Journal of Power Sources 206 (2012) 288–294

Contents lists available at SciVerse ScienceDirect

Journal of Power Sources

journal homepage: www.elsevier.com/locate/jpowsour

Hierarchically textured $Li_xMn_{2-y}O_4$ thin films as positive electrodes for lithium-ion batteries

Martin Bettge[a], Seung Yoon Ryu[b], Scott MacLaren[b], Steve Burdin[b], Ivan Petrov[b], Min-Feng Yu[c], Ernie Sammann[b], Daniel P. Abraham[a,*]

[a] Chemical Sciences and Engineering Division, Argonne National Laboratory, 9700 S. Cass Ave., Argonne, IL 60439, USA
[b] Frederick Seitz Materials Research Laboratory, University of Illinois at Urbana-Champaign, 104 S. Goodwin Ave., Urbana, IL 61801, USA
[c] Department of Mechanical Science and Engineering, University of Illinois at Urbana-Champaign, 1206 W. Green St., Urbana, IL 61801, USA

ARTICLE INFO

Article history:
Received 8 December 2011
Received in revised form 20 January 2012
Accepted 21 January 2012
Available online 28 January 2012

Keywords:
Lithium manganese oxide
Lithium-ion battery
Nanowire
Impedance spectroscopy
Sputtering
Thin film

ABSTRACT

Hierarchical surface morphologies form when thin films are deposited onto preexisting templates of vertically aligned wires using a line-of-sight deposition method, providing a facile path to experimental battery electrodes with high surface-to-volume ratios. To demonstrate this, we fabricate and electrochemically cycle highly textured thin film electrodes of $Li_xMn_{2-y}O_4$ with large surface-to-volume ratios and low impedance. The active surface area of the electrodes exceeds the area of the substrate by at least a factor of five. This factor is due in part to the textured template, and in part to the effects of local shadowing during line-of-sight film deposition, resulting in a hierarchical surface morphology. The textured electrodes maintain their structural integrity for at least 30 cycles, as shown through microstructural characterization and reversible cycling against metallic lithium over the range of 2.0–4.4 V. In comparison to planar thin film electrodes of equal mass, they also offer a lasting reduction in internal impedance. Overall, textured thin film electrodes of any material are readily fabricated through this templating technique and can be used to improve three-dimensional battery architectures or to simply probe electrochemical surface effects.

1. Introduction

Energy density, power density, and cycle life are important performance characteristics for rechargeable batteries. Unfortunately, improving one often corrupts another, due to intricate physical and chemical constraints [1]. One promising approach to relax these constraints is to employ three-dimensional electrode architectures [2–4]. Such electrode architectures can provide large interfacial-area-to-volume ratios, improving charge transport and diffusion kinetics. Their built-in voids allow also for mechanical strain compensation, preventing structural failure. And while gravimetric and volumetric energy densities are intensive material properties, the areal energy density is not. Thus solid-state thin film batteries may also benefit from three-dimensional, more massive electrodes, provided they allow adequate charge transport [5].

Optimized charge transport for a given electrode requires both a large electrode–electrolyte interfacial area for low charge-transfer resistance, and a straight conduction path normal to the current collector for low electronic resistance. For these reasons, aligned nano- and micron scale wire and pore arrays with high aspect ratios are desirable electrode architectures. However, where the need for high volumetric capacity requires a ratio of filled to void space above unity, wire arrays offer more surface area than pore arrays of the same dimensions, making them the preferred geometry for high-density energy-storage applications.

Here, we use vertically aligned, chemically robust silicon oxide nanowires as templates and mechanical support for electrochemically active wire arrays made of $Li_xMn_{2-y}O_4$ (LMO). In general, such nanowire templates allow us to readily fabricate textured electrodes of virtually any material using standard deposition techniques and to probe the influence of surface effects on electrochemical performance.

Fig. 1 depicts an example of such textured electrode. The idealized rendering shows a layered thin film covering the support nanowires and the space between them. In contrast to a planar thin film, the surface area of such textured thin film exceeds that of the substrate.

Fig. 1 depicts more specifically that the silica (SiO_x) nanowires are covered by a thin layer of titanium nitride (TiN), followed by the electrochemically active LMO coating. The oxide support array consists of silica nanowires which are grown by a plasma-assisted vapor-liquid-solid (VLS) technique [6]. No lithography is

* Corresponding author. Tel.: +1 630 252 4332; fax: +1 630 972 4406.
E-mail address: abraham@anl.gov (D.P. Abraham).

0378-7753/$ – see front matter © 2012 Elsevier B.V. All rights reserved.
doi:10.1016/j.jpowsour.2012.01.128

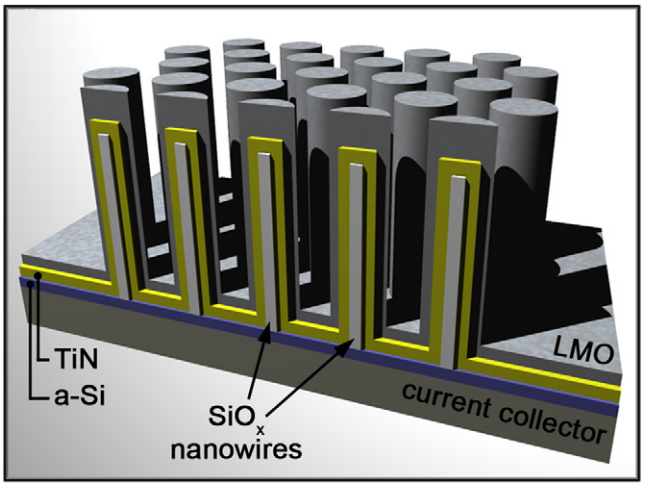

Fig. 1. Idealized rendering of a textured thin film electrode made of $Li_xMn_{2-y}O_4$ (LMO) and supported by oxide nanowires. An intermediate conductive layer of titanium nitride (TiN) is employed to enhance electronic conductivity along the wire axes. An optional thin layer of amorphous silicon (a-Si) is used to provide a controlled surface for oxide nanowire growth on the stainless steel current collector.

carried out, and substrate temperatures remain entirely below 200 °C throughout wire and film growth. Individual nanowires are free-standing and can reach heights up to 10 μm with a mean spacing of less than a few micrometers. Experimental details are provided in Section 2.1 and a more thorough discussion of this growth technique can be found in an earlier publication [6]; however, an array of vertically aligned nanowires made by any other technique could be used instead. The electronically conductive TiN intermediate layer is particularly important underneath low-conductivity films with high aspect-ratio features to improve current collection. It is a material of choice here because of its metallic nature and its chemical stability against lithium [2,7,8].

No particular effort was made to optimize the electrode performance, minimize fabrication cost, or otherwise consider engineering aspects of electrode design for this demonstration. But the choice of LMO as the electrochemically active material was easy because of its many attractive properties. Its theoretical lithium capacity is high and on the order of 200–300 mAh-g^{-1} when cycled over the range of 2.0–4.4 V versus metallic lithium. It is relatively inexpensive and its major component, manganese, is abundant and non-toxic [9,10]. In addition, LMO allows us to effectively probe the electrochemical effects of large surface-to-volume ratios because the ionic conductivity of LMO is significantly lower than its electronic conductivity [9].

LMO nanowires have been previously grown using multiple solution-based processing steps [11,12], or via solid-state reaction [13]. Here, however, we simply rely on the nanowire template to control the topography, and apply the LMO by radio-frequency (RF) magnetron sputtering, a technique previously used for depositing planar LMO films [9,14]. In our approach, the directional nature of the deposition creates nanometer-scale roughness along the wire walls due to glancing angle shadowing. The combination of micrometer texture formed by the nanowire array together with nanometer-scale roughness considerably increases the electrode surface area, while the vertical alignment maintains uniform coverage of the template wires, reducing flexing of the composite elements during cycling. Thus, by adjusting the deposition parameters and template geometries, a wide range of surface-to-volume ratios can be obtained for a wide range of materials through this technique.

2. Experimental

2.1. Growth of supporting silicon oxide nanowires

The supporting oxide nanowire arrays are grown by the plasma-assisted VLS method described previously [6]. Some variations are implemented to promote more uniform nanowire growth, higher aspect-ratio structures, and higher growth rates: A 50 nm thin layer of amorphous silicon (a-Si) is applied to each polished stainless steel substrate by DC magnetron sputtering prior to the application of the indium film that seeds oxide nanowire growth. This silicon layer promotes more uniform indium dewetting. The subsequent nanowire growth is carried out in a magnetron sputtering system with an additional, externally applied magnetic field for improved control of the ion-to-neutral flux ratio during deposition [15]. To grow the oxide nanowire arrays, atomic silicon is sputtered from an undoped silicon magnetron target in an atmosphere containing only argon (700 mPa) and water vapor (3.0–4.0 mPa). The chamber base pressure is 1×10^{-6} Pa. The DC magnetron is operated at a power of 14 W and the substrate is held at a temperature of 175 °C (measured by K-type thermocouple attached to the growth surface). A substrate bias of −500 V is applied to induce energetic ion bombardment at the substrate surface. The magnetic field in the vicinity of the sample is about 100 Gauss increasing plasma density and thus ion flux to the substrate surface during sputter deposition. According to plasma probe measurements, the ion flux is about 0.1 mA-cm^{-2} with average ion energies of approximately 500 eV [15].

2.2. Fabrication of vertically aligned LMO wire arrays

The growth of the silicon oxide nanowires is followed by an application of a thin metallic, chemically stable conformal coating of titanium nitride (TiN) onto the arrays preceding the LMO deposition [8,16]. Due to metallic nature of TiN (40–500 μΩ-cm [7]), the electronic resistance along the nanowire axis can be lowered, even after sample handling in air prior to the LMO deposition. In comparison to TiN, LMO exhibits a relatively high electronic resistivity (~100 kΩ-cm) [9]. TiN is reactively deposited in a mixture of nitrogen (7 mPa) and argon (770 mPa) using an elemental titanium sputter target (Kurt J. Lesker, 99.995%). The DC magnetron is operated at 100 W while the substrate remains close to room temperature. The floating potential of the ungrounded substrate holder is −20 V indicating a moderate-intensity, low-energy ion bombardment. This eases reactive growth of TiN and improves conformal coverage during directional deposition onto high aspect ratio structures [16,17].

As grown, the silicon oxide nanowires are typically slightly tapered and spaced 1–2 μm apart, providing a good template for conformal line-of-sight deposition. The average areal density is 0.3 wires-μm^{-2}. A continuous coating is essential to ensure uninterrupted charge transport from the wire to the current collecting substrate. Continuity of the TiN coating is improved by periodically tilting the sample stage during deposition by a small angle, covering the range of about ±10°, depending on mean height and spacing of the supporting oxide nanowires. If deposited onto a smooth planar substrate, the TiN film thickness is 85 nm. When deposited onto the nanowire array, the characteristic thickness of the layer, i.e. its volume divided by surface area, becomes 29 nm, as estimated using a cylindrical-wire model of the array with dimensions from SEM observations.

Following the TiN deposition, a thicker LMO coating is applied by RF magnetron sputtering from two commercial targets, each 5 cm in diameter, located at the same distance from the $LiMn_2O_4$ substrate (Super Conductor Materials, Inc., 99.9%) in an argon (190 mPa) and oxygen (13 mPa) atmosphere with the substrate close to room

Table 1
Characteristics of LMO thin film electrodes.

Material	Type	Calculated total mass (mg)	Surface area[a] (cm^2)	Characteristic thickness[b] (nm)	1st charge gravimetric capacity (mAh-g^{-1})
LMO	Planar	0.15	1.97	180	205.2
LMO	Textured	0.15	9.2	40	231.4

[a] Minimum surface area is calculated assuming a smooth thin film for planar films; and using a cylindrical rod array for textured films, with mean height, width, and spacing of the wires determined by scanning electron microscopy (SEM). Nanoscale surface roughness is not considered.
[b] Characteristic thickness is defined as volume divided by surface area.

temperature. The floating potential of the ungrounded substrate holder is −26 V, again indicating moderate-intensity, low-energy ion bombardment. A planar LMO reference film deposited on a silicon substrate exhibits no crystalline phases by ω–2θ and glancing angle X-ray diffraction scans, however grain sizes of about 5 nm are apparent in high-resolution TEM (Section 3.2). The Li/Mn ratio of this reference film is ∼1, measured by inductively coupled plasma atomic spectroscopy (ICP). This relatively high ratio has been previously observed for sputter deposited films from $LiMn_2O_4$ targets and has been found to decrease with higher deposition rates and lower O_2/Ar ratios [9]. In our case, the deposition rate is relatively low (0.4 nm-min^{-1}), in part because the target-substrate distance of 15 cm is large compared to the diameter of the targets. The continuity of this film is again improved by periodically tilting the sample stage. If deposited onto a smooth planar substrate, the LMO film is 180 nm thick. If deposited onto the nanowire array the characteristic thickness becomes 40 nm with a surface area of at least 9.2 cm^2. This is an increase in surface area by 4.7 times relative to a planar film. The surface area is estimated based on a cylindrical rod array with mean height (10 μm), width or diameter (0.35 μm), and spacing (0.3 wires-μm^{-2}) of the LMO wires, as determined by SEM. This surface area is underestimated as it does not include the observed nanoscale roughness (Section 3.2).

2.3. Fabrication of planar LMO samples

Fabrication of the planar samples is carried out using the same experimental apparatus as mentioned for the LMO wire arrays, without the intermediate processing steps of indium seed layer deposition and oxide nanowire growth. The same initial layers, of 50 nm silicon and 85 nm TiN, are deposited on each control sample substrate to ensure the closest possible similarity to the textured films. The final deposition of LMO is done under the same sputtering conditions as for the textured films.

2.4. Microstructural and chemical characterization

Microstructural characterization is carried out using scanning and transmission and electron microscopy (SEM, TEM), and X-ray diffraction (XRD). XRD experiments are conducted with a Philips X'pert MRD; glancing angle (1°) and $\omega - 2\theta$ scans covering the range of 20–88° with 2 s and 0.05 degrees per step, respectively, using an X-ray wavelength of 1.5418 Å (CuKα). For SEM a high-resolution Hitachi-4800 is used. The TEM experiments are conducted on a JEOL 2010LaB6 and a JEOL 2010F; the latter instrument is also used to provide selected-area energy dispersive X-ray spectroscopy (Oxford INCA_EDS detector) for elemental analysis.

2.5. Electrochemical characterization of planar and textured electrodes

To study the electrochemistry of textured LMO, control samples and textured films are deposited on mirror-polished stainless steel coins that act as current collectors and can readily be integrated into standard 2032-type coin cells with metallic lithium counter electrodes. Each control sample consists of a planar thin film with the same mass, 0.15 mg, as that of its textured counterpart. To ensure equal mass, textured and planar films are deposited under identical conditions at a known deposition rate. The film density for LMO is assumed to be 4.2 g-cm^{-3} [9]. Cells are assembled in an argon-filled glove box. However, the LMO electrodes were exposed to air without bakeout prior to cell assembly. The electrode area is 1.97 cm^2. The electrolyte contains 1.2 M $LiPF_6$ in an ethylene carbonate (EC): ethyl methyl carbonate (EMC) (3:7 by wt.) solvent. A separator (Celgard 2325) provides electronic isolation between the electrodes. The planar and textured LMO electrodes are cycled between 4.4 V and 2.0 V at a rate of 20 mA-g^{-1}; further details are summarized in Table 1. Electrochemical characterization includes capacity, cycling, and electrochemical impedance spectroscopy (EIS) measurements at 30 °C. The EIS measurements are conducted with an EG&G 273A potentiostat and a Solartron SI1260 Frequency Response Analyzer controlled by ZPLOT measurement software. The impedance spectra are acquired in the 100 kHz to 10 mHz frequency range with a 10 mV peak-to-peak perturbation around an open-circuit cell potential of 3.9 V. The cells are held at that voltage, using a constant voltage program, for several hours before the EIS measurements.

3. Results and discussion

3.1. Electrochemical performance of highly textured lithium manganese oxide (LMO) electrodes

Arrays of LMO wires are structurally stable under extended cycling and show lower internal impedances than their planar counterparts. Fig. 2A and B depict the wire morphology before and after electrochemical cycling, respectively. After 30 cycles over a range of 2.0–4.4 V, the free-standing nature of the wires is well preserved; detachment of individual wires is only occasionally observed. Possible causes for detachment include excessive mechanical strains during cycling, shear forces introduced during cell assembly, disassembly, and final electrode rinsing. The wire diameters, around 300 nm, remain unchanged, after electrochemical cycling. The structural integrity of the electrode was further confirmed by TEM (Section 3.2.).

Fig. 3A shows the relative capacity retention of an LMO wire array versus that of a planar LMO thin film. The textured electrode exhibits a gradual capacity fade of about 0.4% from the third cycle on, whereas the planar electrode retains its initial capacity well. The reason for the capacity fade is not clear: SEM and TEM indicate that the wire morphology is largely preserved, yet occasional wire detachment could certainly be the underlying cause for this capacity fade. Also, the impedance of the textured films is lower than that of the planar ones and thus cannot contribute to the capacity fade (details are given in the following paragraphs). The capacity fade could also be caused by chemical dissolution of manganese cations which has been reported to occur primarily at elevated potentials (>4.1 V) and to scale well with electrode–electrolyte interfacial areas [10,18,19]. Water contamination of the electrolyte could further enhance such dissolution [20]. Other causes include structural changes and/or other loss mechanisms within the complex oxide [21,22]. Surface modification of the oxide cathode is one possible

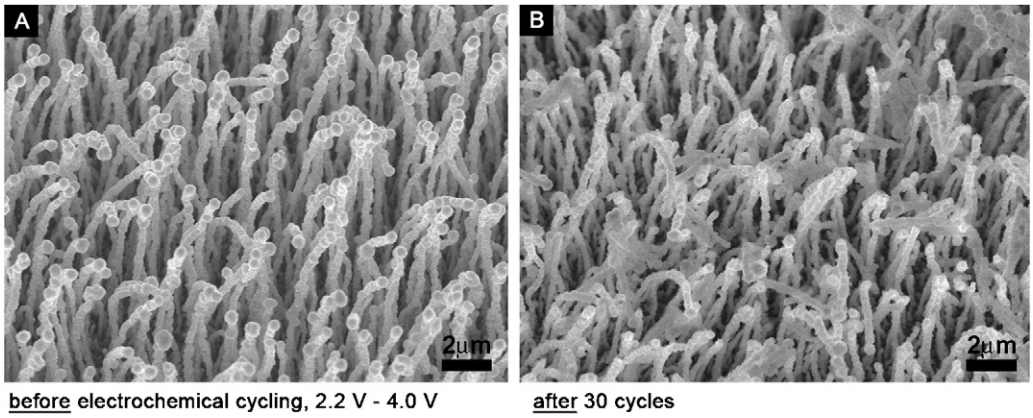

Fig. 2. SEM micrographs of the textured $Li_xMn_{2-y}O_4$ electrodes before electrochemical cycling (A) and after 30 charge and discharge cycles between 2.2 V and 4.0 V (B). The scale bars represent 2 μm; substrate tilt during SEM is 30°.

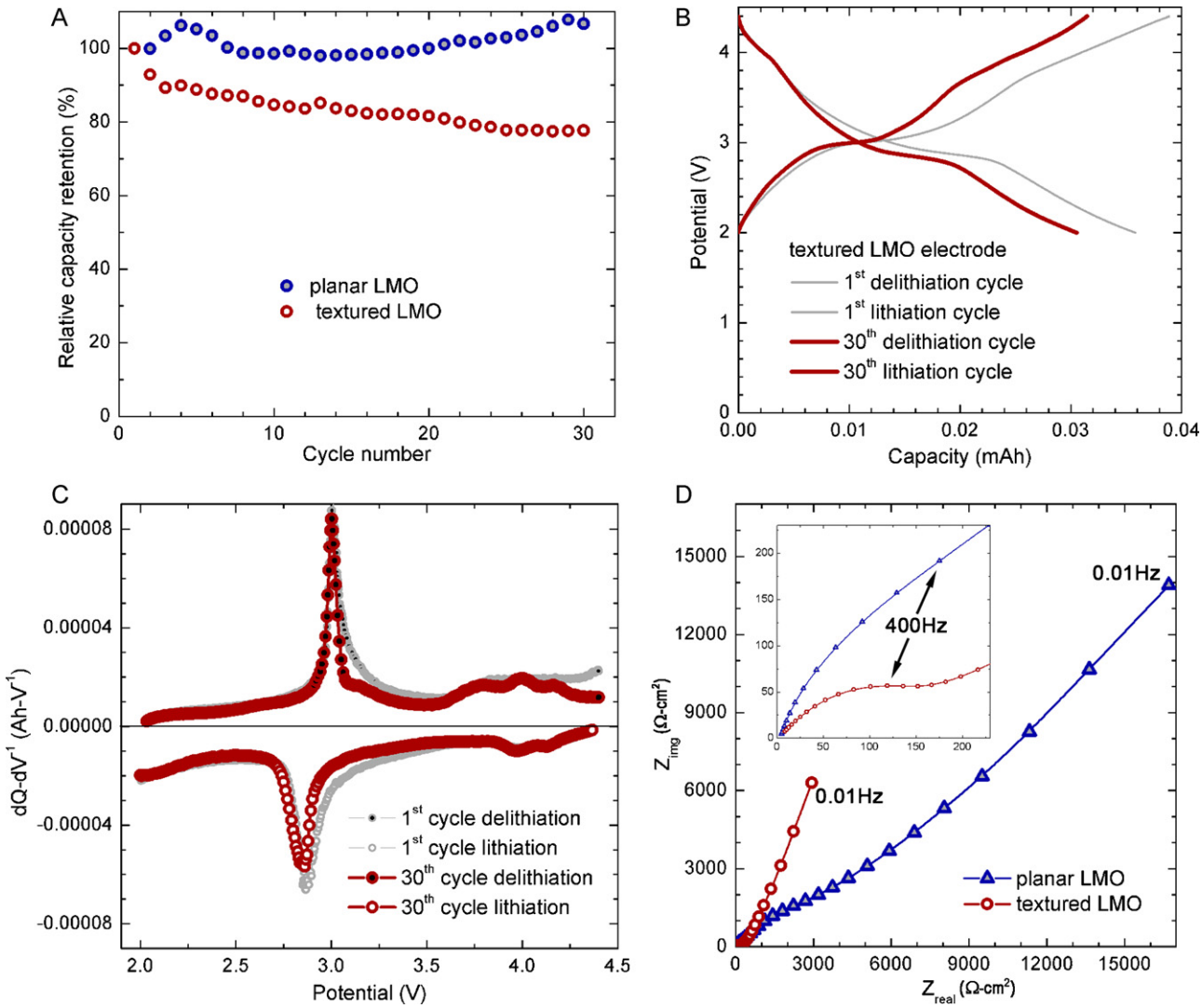

Fig. 3. Electrochemical characterization of textured and planar LMO thin film electrodes. The weight of each electrode is 0.15 mg; the area of the substrates 1.97 cm^2. (A) Relative capacity retention of a planar and a textured LMO thin film; (B) Constant-current potential profile for a textured LMO thin film during 1st and 30th cycle; (C) Differential capacity (dQ/dV) profile for a textured LMO thin film during 1st and 30th cycle; (D) Area-specific complex impedance (referred to substrate area) of a planar and a textured LMO thin film, after 30 cycles at 3.9 V during lithiation (discharge).

route to prevent or reduce some of the suggested loss mechanisms [10,18,22].

Fig. 3B and C display the potential and the differential capacity (dQ/dV) profiles for a textured film after the 1st and 30th cycle. The profiles exhibit characteristic features for sputter-deposited $Li_xMn_{2-y}O_4$ (for $\sim 2 \geq x \geq \sim 1$) and are different from those of $Li_xMn_2O_4$ spinel powders synthesized by other methods. Highly crystalline $Li_xMn_2O_4$ undergoes over this range two major plateaus in its potential profile, or peaks in its dQ/dV profile [21]. During discharge, one plateau is located around 4 V and is attributed to lithium ion removal from the tetrahedral spinel sites. Close inspection of this plateau shows in fact two separate sloping regions, revealing lithium ordering on those sites. The other major plateau is located just below 3 V and is attributed to a first-order phase transition from the $LiMn_2O_4$ spinel to the $Li_2Mn_2O_4$ rock salt composition.

In contrast, the sputter-deposited films barely show a 4 V sloping region, indicating a lack of lithium ions on tetrahedral sites. Similar electrochemical behavior has also been reported by Dudney et al. and may indicate a typical behavior for LMO films sputter deposited at low temperatures and rates [9]. To explain the difference between sputter-deposited films and highly crystalline $LiMn_2O_4$, Thackeray proposed a structure of two intergrown spinels that would reduce the number of lithium ions on the tetrahedral sites, and thus the capacity in the 4 V region [21]. The potential profiles of our planar films, not shown here, showed similar features. In general, though, the open-circuit voltages are 3.2 V for the as-deposited planar films and 2.0 V for the as-deposited textured films, suggesting higher lithium content in the textured electrodes.

The most striking feature, however, is the relatively low impedance of textured LMO electrodes in comparison to that of planar ones at all frequencies (Fig. 3D). In fact, this is expected as charge-transfer and diffusion impedances are lower for textured electrodes due to the larger surface-area-to-volume ratio. The complex impedance plots of a textured and a planar electrode in Fig. 3D are taken after 30 cycles at 3.9 V during lithiation. For the textured electrode, the plot shows (a) a high-frequency resistance ($Z_{real} = 8.5\,\Omega$ at 100 kHz vs. 5 Ω at 100 kHz for the planar sample; neither appears to have reached the asymptotic minimum by 100 kHz although the planar sample comes close) that includes contributions from the measurement instrumentation (typically several ohms), (b) a mid-frequency arc related to electrode-electrolyte interfacial processes, and (c) a low-frequency sloping line (Warburg tail), at frequencies less than ~10 Hz. We also estimate the charge-transfer (CT) resistances by fitting the arc with a semicircle. This assumes resistive and capacitive behavior in parallel for the CT phenomena at the electrode–electrolyte interface. For the textured electrode, the arc intersection with the real impedance axis gives a CT resistance of about 236 Ω-cm^2 with a maximum imaginary part, i.e. $\omega RC = 1$, at a frequency of 400 Hz. For the planar electrode, we estimate this resistance to be roughly on the order of 3 kΩ-cm^2.

Charge transport is diffusion-limited in both electrode types at the lower frequencies, where the sloping line which is typically associated with diffusion phenomena through the electrolyte and active material dominates the impedance curves [23,24]. But the relative importance of diffusion processes is greater in the planar electrode, as evident from the partial disappearance of its mid-frequency arc [24]. To demonstrate the low-frequency impedance scaling with surface area, the magnitudes of the area-specific impedances of the two electrode types are normalized to the surface area of the substrate and plotted in Fig. 4. At 10 Hz, the magnitudes are approximately 280 Ω-cm^2 and 1490 kΩ-cm^2 for the textured and planar electrodes, respectively. As expected, the ratio of these impedances is close to the inverse of the ratio of the predicted electrode surface areas. At equal volume, the surface area of a textured film is 9.2 cm^2 and thus roughly five times larger than

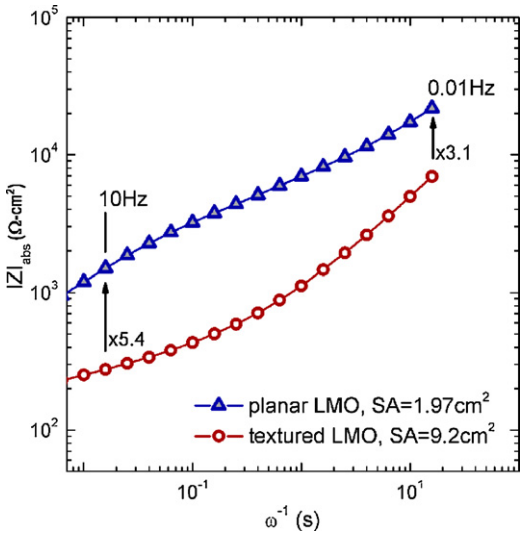

Fig. 4. Magnitudes of the area-specific impedance (referred to substrate area) of planar and textured LMO thin films are plotted as a function of inverse angular frequency in the low-frequency regime. Data are the same as in Fig. 3D. Low frequency impedance is smaller for the textured films than for planar films. The impedance ratio of the electrodes (indicated by numbers close to arrows) agrees well with the inverse ratio of the estimated active surface areas of ~4.7.

that of a planar one (1.97 cm^2), as estimated from basic geometric assumptions. (Note that this factor does not consider the observed nano-scale roughness found during TEM, Section 3.2). Although both impedance magnitudes rise by one to one-half decades as the frequency decreases by three decades, their ratio remains fairly constant over this large frequency span. This behavior is consistent with one-dimensional diffusion in the low-frequency, thick-sample limit, as described by Ho et al. [25].

This discussion of impedance considerations would not be complete without mention of the TiN current collection layer. It is the TiN film that makes the electrically insulating silica template a suitable support for stacking LMO above the plane of the substrate. Without it, electrical connection to the stacked active material would pass through the length dimension of the high-resistivity LMO, rather than through its much smaller thickness.

The electrical resistance of the TiN pathway is best observed in the high-frequency limit, where the sum of the capacitive reactance of the LMO and of the charge transfer layer approaches zero (i.e., a short circuit). In that limit, the TiN layers coating the template wires act as an array of resistors, wired in parallel, connecting the electrolyte to the substrate. An upper bound on the resistance of one such TiN film, from tip to base of the wire, is $R_{TiN} = L\rho_{TiN}/\pi b t_{TiN}$, where L is the length of the wire, b is the radius of the interface between the TiN and LMO layers, and for the TiN film, t_{TiN} is the thickness and ρ_{TiN} the resistivity. Given n such resistors in parallel per unit area, the TiN component of the high-frequency limit of the area-specific electrode resistance will not exceed $R_P = L\rho_{TiN}/n\pi b t_{TiN}$. The actual resistance must be less than this, since the current enters the wires over their entire lengths, not just at the tips. Given the deposition conditions already described, with b in excess of 10 nm, t_{TiN} on the order of 4 nm, n on the order of 0.3 μm^{-2}, L equal to 10 μm, and using a relatively high 1 mΩ-cm for ρ_{TiN} [7], R_P should be no greater than 2 μΩ-cm^2, or about 1 μΩ over the 1.6 cm^2 electrode area. Any impedance penalty caused by the use of electrically insulating template wires is clearly negligible. The 3.5 Ω difference in high frequency resistance observed between the planar and textured cells is thus likely to arise from other causes, not the least of which is the fact that the 100 kHz impedance data do not represent the asymptotic high-frequency limits for the two electrode types.

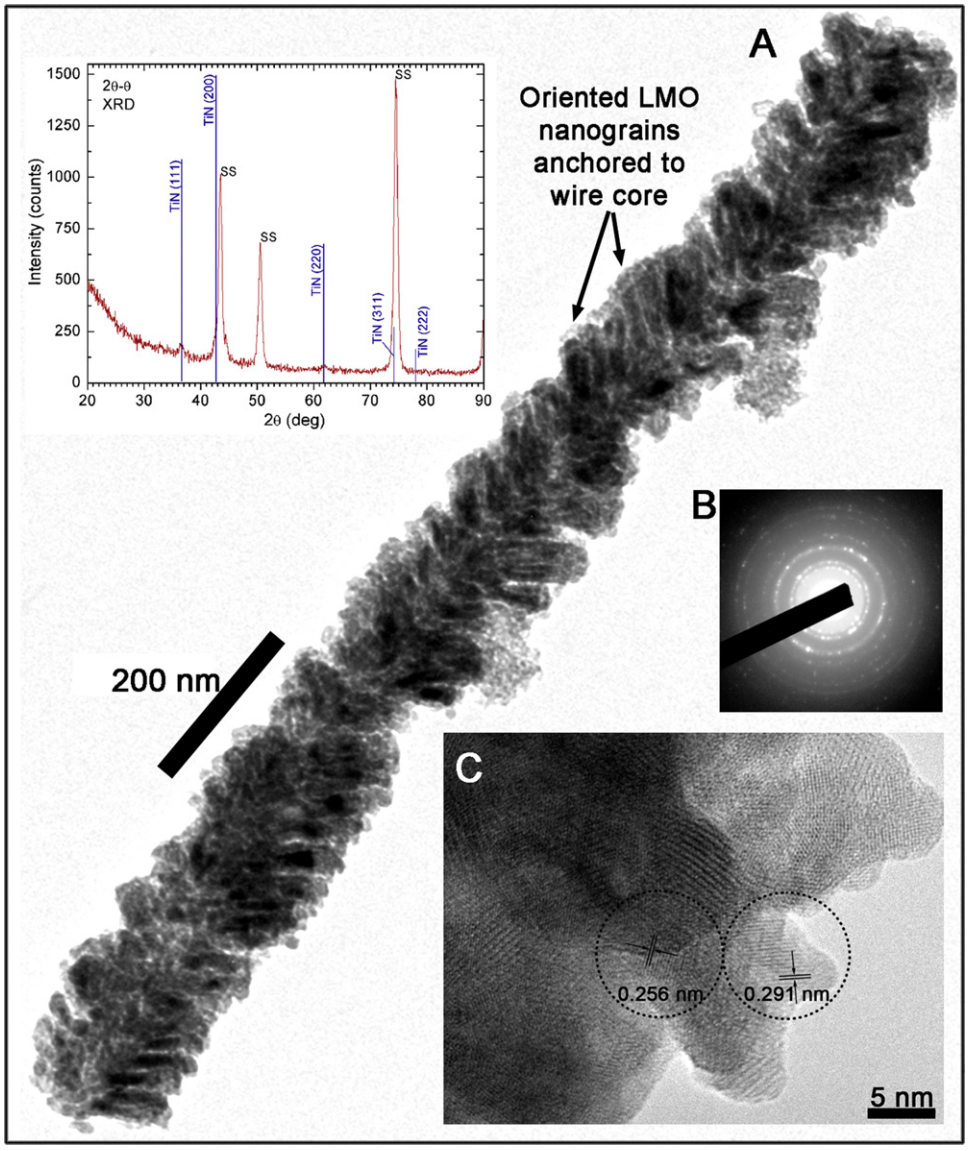

Fig. 5. (A) An individual wire covered with a $Li_xMn_{2-y}O_4$ thin film after 30 cycles of lithiation and delithiation. The LMO film consists of oriented nanograins anchored to the wire's core. Some organic residue is found to adhere to the wire's outer surface. The top-left inset shows an $\omega - 2\theta$ XRD scan of the entire thin film electrode. Crystalline peaks of TiN and the stainless steel substrate are identified. TiN is used as a conductive layer beneath the LMO, surrounding the amorphous silicon oxide core. (B), (C) Selected-area electron diffraction pattern and high-resolution TEM taken at the outermost sidewall reveal a nanocrystalline LMO thin film with grain sizes of around 5 nm.

3.2. Microstructural characterization of highly textured lithium manganese oxide electrodes

Structure and composition are examined by X-ray diffraction (XRD), SEM, TEM and energy-dispersive X-ray analysis (EDX) (Figs. 5 and 6). Fig. 5A shows a TEM overview of a typical core-shell electrode wire. A fine-grained surface with nanoscale roughness is clearly visible. Thickness and nature of the coating is quite consistent over this entire wire section which is approximately 1.5 μm long. The core of this wire can be regarded as an axial "anchor-line" for the outward oriented nanosized grains. These nanograins appear to be aligned and oriented along a ∼45° angle with respect to the wire axis. Such grain orientation is characteristic for thin films grown via glancing angle deposition (GLAD) [26]. The LMO films here are deposited via magnetron sputtering which is a "line-of-sight" physical vapor deposition technique. Since the wires are vertically aligned and thus oriented along the direction of the incoming flux, deposition onto the outer wire surfaces is GLAD-like and induced by local shadowing intensifying as deposition continues. If surface adatom mobility is sufficiently low, films grown via GLAD are highly columnar and underdense [26]. The growth of such aligned nanograins along the outer wire sidewalls increases the overall electrode surface area. A lower bound estimate, based on the measured length and orientation of the nanograins, suggests an additional increase in surface area by at least 2–3 times due to this nanoscale roughness. Despite deposition at room-temperature and electrochemical cycling, the active LMO thin film is crystalline. In Fig. 5B, ring patterns from selected-area electron diffraction (SAED) reveal the material's nanocrystallinity. In Fig. 5C, the bright-field high-resolution TEM reveals grain sizes on the order of 5 nm.

The presence and stability of the intermediate TiN layer after cycling is verified by a large area $\omega - 2\theta$ XRD scan displayed in the upper left inset of Fig. 5. The dominant diffraction peaks are related to the stainless steel substrate (SS), while the minor peaks are related to the NaCl-structure of TiN (powder diffraction file 04-008-7173). The LMO peaks are not apparent in the XRD data partly because of the nanocrystalline nature of the material.

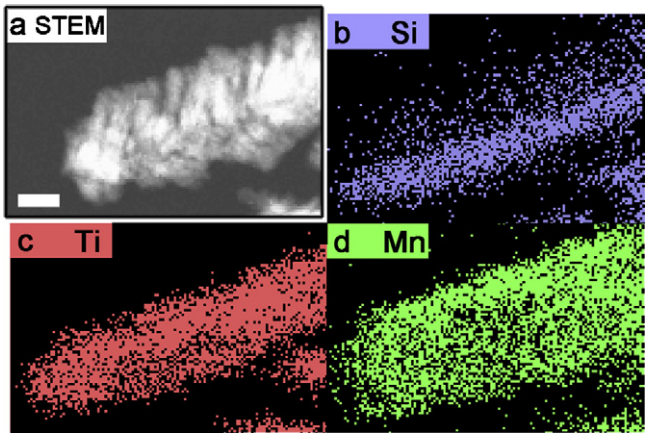

Fig. 6. Scanning TEM (STEM) and elemental EDX mapping of an individual electrode wire. (A) STEM on section of wire. The scale bar corresponds to 75 nm. (B)–(D) Spatial EDX mapping of silicon, titanium, and manganese, respectively. The layered core-shell structure of the wire appears to remain intact throughout cycling – with silicon oxide as core material, and titanium nitride and $Li_xMn_{2-y}O_4$ as materials for the second and third shells, respectively.

Fig. 6 demonstrates that the layered core–shell structure (SiO_x/TiN/LMO) appears to remain intact after cycling as confirmed by elemental EDX mapping inside the TEM. In Fig. 6A, a section of the wire is displayed as a spatial reference for the subsequent elemental mapping of silicon, titanium, and manganese (Figs. 6B–D, respectively). Here, the spatial distribution of silicon, titanium, and manganese correspond to the presence of silicon oxide, TiN, and LMO which are the primary components of the core, the intermediate, and the outer shell. It is evident from Figs. 6B–D that the spatial distribution for manganese, taken perpendicular to the wire axis, is wider than that for titanium; and that the spatial distribution for titanium is wider than that for silicon. The small difference in wire location between the STEM image in Fig. 6A and Figs. 6B–D is caused by sample drift during TEM mode switching.

4. Conclusions

Fabrication and electrochemical performance of hierarchically textured thin film electrodes of nanocrystalline lithium manganese oxide ($Li_xMn_{2-y}O_4$) is demonstrated. We achieve texturing here by using a support template made from free-standing nanowires onto which the electrochemically active material is sputter deposited at room temperature. The nanowire cores are made of silicon oxide; and a thin coating of metallic titanium nitride (TiN) provides adequate adhesion of the active material and sufficient electronic conductivity along the nanowire axes throughout cycling. The effects of local shadowing upon line-of-sight thin film deposition trigger columnar growth of the active material and thus create a hierarchical surface morphology down to the nanoscale. After 30 cycles, the textured electrodes maintain their structural integrity and have a capacity of around 200 mAh-g^{-1} or 15 μAh-cm^{-2} over the range of 2.0–4.4 V versus lithium. Despite some observed capacity fade, they exhibit low-frequency diffusion impedances that are roughly one-fifth that of planar electrodes of equal mass. This is in good agreement with the estimated lower bound surface area that is about 5 times larger than that of a planar electrode.

Acknowledgments

The submitted manuscript has been created by UChicago Argonne, LLC, Operator of Argonne National Laboratory ("Argonne"). Argonne, a U.S. Department of Energy Office of Science laboratory, is operated under Contract No. DE-AC02-06CH11357. We acknowledge use of the Frederick Seitz Materials Research Laboratory Central Facilities, University of Illinois; this facility is supported by the U.S. Department of Energy under grants DE-FG02-07ER46453 and DE-FG02-07ER46471. We thank Prof. John A. Rogers for helpful discussions and for providing some of the sputter targets used in this study. We would like to further extend our gratitude to the following individuals: Stephen E. Trask who helped to assemble and cycle the electrochemical test cells; and Brandon Howe, Jian-Guo Wen, and Mauro Sardela who helped to deposit and characterize the textured thin films.

References

[1] J.W. Long, B. Dunn, D.R. Rolison, H.S. White, Chem. Rev. 104 (2004) 4463.
[2] L. Baggetto, R.A.H. Niessen, F. Roozeboom, P.H.L. Notten, Adv. Funct. Mater. 18 (2008) 1057.
[3] C.K. Chan, H. Peng, G. Liu, K. McIlwrath, X.F. Zhang, R.A. Huggins, Y. Cui, Nat. Nanotechnol. 3 (2008) 31.
[4] P.L. Taberna, S. Mitra, P. Poizot, P. Simon, J.-M. Tarascon, Nat. Mater. 5 (2006) 567.
[5] F. Xu, N.J. Dudney, G.M. Veith, Y. Kim, C. Erdonmez, W. Lai, Y.-M. Chiang, J. Mater. Res. 25 (2010) 1507.
[6] M. Bettge, S. MacLaren, S. Burdin, J.-G. Wen, D. Abraham, I. Petrov, E. Sammann, Nanotechnology 20 (2009) 115607.
[7] P. Patsalas, S. Logothetidis, J. Appl. Phys. 90 (2001) 4725.
[8] I.s. Kim, P.N. Kumta, G.E. Blomgren, Electrochem. Solid-State Lett. 3 (2000) 493.
[9] N.J. Dudney, J.B. Bates, R.A. Zuhr, S. Young, J.D. Robertson, H.P. Jun, S.A. Hackney, J. Electrochem. Soc. 146 (1999) 2455.
[10] M.S. Whittingham, Chem. Rev. 104 (2004) 4271.
[11] E. Hosono, T. Kudo, I. Honma, H. Matsuda, H. Zhou, Nano Lett. 9 (2009) 1045.
[12] Y.k. Zhou, C.-m. Shen, J. Huang, H.-l. Li, Mater. Sci. Eng. B95 (2002) 77.
[13] H-W. Lee, P. Muralidharan, R. Ruffo, C.M. Mari, Y. Cui, D.K. Kim, Nano Lett. 10 (2010) 3852.
[14] K.-F. Chiu, H.C. Li, K.M. Li, C.H. Tsai, J. Electrochem. Soc. 152 (2005) A2058.
[15] I. Petrov, F. Adibi, J.E. Greene, W.D. Sproul, W.-D. Münz, J. Vac. Sci. Technol. A 10 (1992) 3283.
[16] L. Hultman, J.-E. Sundgren, J.E. Greene, D.B. Bergstrom, I. Petrov, J. Appl. Phys. 78 (1995) 5395.
[17] S. Hamaguchi, S.M. Rossnagel, J. Vac. Sci. Technol. B 13 (1995) 183.
[18] G. Amatucci, A. Du Pasquier, A. Blyr, T. Zheng, J.-M. Tarascon, Electrochim. Acta 45 (1999) 255.
[19] D.H. Jang, Y.J. Shin, S.M. Oh, J. Electrochem. Soc. 143 (1996) 2204.
[20] D.H. Jang, S.M. Oh, J. Electrochem. Soc. 144 (1997) 3342.
[21] M.M. Thackeray, Prog. Solids Chem. 25 (1997) l.
[22] K.A. Walz, C.S. Johnson, J. Genthe, L.C. Stoiber, W.A. Zeltner, M.A. Anderson, M.M. Thackeray, J. Power Sources 195 (2010) 4943.
[23] D.P. Abraham, S.D. Poppen, A.N. Jansen, J. Liu, D.W. Dees, Electrochim. Acta 49 (2004) 4763.
[24] E. Barsoukov, in: E. Barsoukov, J.R. MacDonald (Eds.), Impedance Spectroscopy – Theory, Experiment, and Applications, 2nd ed., John Wiley, New Jersey, 2005, Ch. 4.5.
[25] C. Ho, I.D. Raistrick, R.A. Huggins, J. Electrochem. Soc. 127 (1980) 343.
[26] M.M. Hawkeye, M.J. Brett, J. Vac. Sci. Technol. A 25 (2007) 1317.